Engineering two-mode interactions in ion traps

J. Steinbach, J. Twamley, and P. L. Knight
Optics Section, Blackett Laboratory, Imperial College, London SW7 2BZ, United Kingdom
(Received 8 April 1997)

We describe how two vibrational degrees of freedom of a single trapped ion can be coupled through the action of suitably chosen laser excitation. We concentrate on a two-dimensional ion trap with dissimilar vibrational frequencies in the x and y directions of motion and derive from first principles a variety of quantized two-mode couplings, concentrating on a linear coupling that takes excitations from one mode to another. We demonstrate how this can result in a state rotation, in which it is possible to transfer the motional state of the ion from, say, the x direction to the y direction without prior knowledge of that motional state. [S1050-2947(97)05711-9]

PACS number(s): 03.75.Be

I. INTRODUCTION

In recent years, advances in the cooling and trapping of ions have led to a situation in which the center-of-mass (c.m.) motion of trapped ions has to be treated quantum mechanically [1]. This motion can be coherently controlled by coupling the ion's external and internal degrees of freedom through laser irradiation [2–6]. Systems of trapped ions have been employed to demonstrate experimentally the generation and measurement of nonclassical states of the ion's c.m. motion [7–10]. Furthermore, trapped ions have been used to implement quantum logic gates [11–13].

Most of the previous investigations have focused on the one-dimensional quantum motion of trapped ions. Recently, Gou *et al.* [14–18] considered the generation of particular two-mode states of an ion. In this paper we address the issue of how to engineer a class of interactions between two of the quantized motional degrees of freedom of a single trapped ion. We assume that the ion is confined within a trap potential that can be closely approximated by a two-dimensional harmonic well. In this case the c.m. motion of the ion is completely equivalent to that of a two-dimensional harmonic oscillator, characterized by two frequencies of oscillation ν_a and ν_b in orthogonal directions x and y, and the corresponding operators $\hat{a}^\dagger$ ($\hat{a}$) and $\hat{b}^\dagger$ ($\hat{b}$) create (annihilate) vibrational excitations in the x and y directions. The interaction that we want to engineer is of the parametric form

$$\hat{H}_I = \hbar\{g\hat{a}^{\dagger k_a}\hat{b}^{k_b} + g^*\hat{a}^{k_a}\hat{b}^{\dagger k_b}\}, \tag{1}$$

where k_a and k_b are positive integers and g is a complex coupling constant. In particular, we note that the powers k_a and k_b can be independently controlled to take on any positive integer numbers and the phase of the coupling constant g is freely adjustable. To give specific examples of this class of interaction between the two vibrational modes a and b, we address the two coupling Hamiltonians

$$\hat{H}_I^{(1)} = i\hbar g\{\hat{a}^\dagger\hat{b} - \hat{a}\hat{b}^\dagger\}, \tag{2}$$

$$\hat{H}_I^{(3)} = \hbar\{g\hat{a}^{\dagger 3}\hat{b} + g^*\hat{a}^3\hat{b}^\dagger\}. \tag{3}$$

The Hamiltonian (2) generates an active rotation of the two-dimensional quantized motional state of the ion at a frequency g, where g is real. Here $\hat{H}_I^{(1)}$ is the kind of Hamiltonian associated with a linear coupler or beam splitter in optics (see, e.g., [19] and references therein). There a photon in mode a is annihilated and a photon in mode b is created, and vice versa. In a trapped ion, vibrational anticorrelated SU(2) states of motion characteristic of this kind of linear coupling can be generated [14]. The linear coupling $\hat{H}_I^{(1)}$ makes it possible to transfer the motional state of the ion from, say, the x direction into the y direction *without prior knowledge* of that motional state and irrespective of whether it is a pure or a mixed state. In the situation in which one may want to use the quantized motion in the x direction for quantum computation [11–13], perhaps later entangling the quantum state of motion with internal electronic states, the y direction can then be employed as a quantum memory element. Note the key point here is that states of motion in the x direction can be transferred entirely to the y direction without reading out their nature entirely nondestructively. The Hamiltonian $\hat{H}_I^{(3)}$ is of the three-photon down-conversion kind: In optics, it represents a process in which one pump photon in mode b is annihilated and three photons in mode a are created, and vice versa. This process is known to be highly peculiar: Unlike its two-photon down-conversion counterpart, quantization of the pump is essential to avoid pathological divergences [20]. These are avoided in a fully quantized treatment, where the pump and down-converted field modes become highly entangled [21].

In Sec. II we first introduce a two-mode Raman transition that couples the electronic and motional degrees of freedom of the ion. Choosing the initial state of the ion to be a direct product of an arbitrary motional state and a specific electronic state, we then decouple the electronic and motional dynamics of the ion through a particular configuration of laser beams (Sec. III). In the Lamb-Dicke approximation and in the limit of suitable trap anisotropy we obtain the above Hamiltonian (1) for various sideband detunings of the lasers. We then examine the severity of the approximations made to obtain the Hamiltonian (1). In Sec. IV we obtain analytical estimates regarding the effects of off-resonant and higher on-resonant processes. In Sec. V we specialize to the case

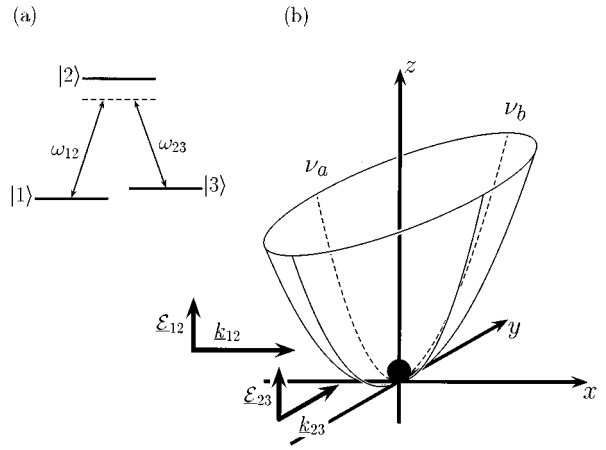

FIG. 1. Two-mode Raman transition that couples the electronic and the two motional degrees of freedom in the x and y directions. The effective three-level ion shown in (a) is confined within a two-dimensional harmonic trap. As illustrated in (b), two laser beams propagating in the x and y directions generate a stimulated Raman transition between the ground states $|1\rangle$ and $|3\rangle$.

$k_a = k_b = 1$ and show that the Hamiltonian $\hat{H}_I^{(1)}$ rotates the motional quantum state of the ion. Finally, we perform a numerical analysis of the complete quantum dynamics and find that the Hamiltonian (2) can be accurately engineered over a range of parameters.

II. GENERAL TWO-MODE RAMAN COUPLING

In the following we describe the Raman coupling that we use to engineer the Hamiltonian given in Eq. (1). We consider an effective three-level ion in a Λ configuration, confined within a two-dimensional harmonic trap as illustrated in Fig. 1. The trap is characterized by the two frequencies ν_a and ν_b, which describe the harmonic potential in the x and y directions, respectively. As shown in Fig. 1, the ion is excited by two linearly polarized laser beams that propagate in the x and y directions connecting levels $|1\rangle \Leftrightarrow |2\rangle$ and $|2\rangle \Leftrightarrow |3\rangle$. These beams are far detuned from the excited state $|2\rangle$ in order to generate a stimulated Raman transition between the two states $|1\rangle$ and $|3\rangle$. We assume states $|1\rangle$ and $|3\rangle$ to be ground-state hyperfine sublevels.

We do not include decoherence effects in our model for the following reason. The Raman coupled energy-level scheme greatly suppresses the spontaneous emission between the two ground-state levels $|3\rangle$ and $|1\rangle$ as these states are coupled by $M1$ and $E2$ transitions at best. At the same time we neglect the effects of spontaneous emission from level $|2\rangle$, as the coupling to the excited state can be effectively eliminated over the time scales of interest to us here when the laser beams are far detuned. Another source of decoherence in ion trap experiments is classical noise in the laser beams and trapping potential. This may be described using so-called intrinsic decoherence models (see, e.g., [22]) of dephasing. The effects of this kind of decoherence have been seen in a recent experiment by Meekhof *et al.* [7]. However, they expect to reduce decoherence from classical noise sources significantly in future experiments [23]. We thus do not include any decoherence effects in our model.

Treating the laser excitations classically, the two electric fields are described by

$$\underline{\mathcal{E}}_{12}(\hat{x},t) = \underline{e}_{12}\{E_{12}e^{-i[k_{12}\hat{x}-\omega_{12}t]} + \text{H.c.}\},$$

$$\underline{\mathcal{E}}_{23}(\hat{y},t) = \underline{e}_{23}\{E_{23}e^{-i[k_{23}\hat{y}-\omega_{23}t]} + \text{H.c.}\}, \tag{4}$$

where $\underline{e}_{12}$ and $\underline{e}_{23}$ are polarization vectors, k_{12} and k_{23} are wave numbers, and ω_{12} and ω_{23} are the frequencies of the lasers. We assume the laser phases to be absorbed in the complex amplitudes E_{12} and E_{23}. In dipole approximation this leads to the Hamiltonian

$$\hat{H} = \hbar\omega_1|1\rangle\langle 1| + \hbar\omega_2|2\rangle\langle 2| + \hbar\omega_3|3\rangle\langle 3| + \hbar\nu_a(\hat{a}^\dagger\hat{a}) + \hbar\nu_b(\hat{b}^\dagger\hat{b}) - \underline{D}_{12}\cdot\underline{\mathcal{E}}_{12} - \underline{D}_{23}\cdot\underline{\mathcal{E}}_{23}, \tag{5}$$

where we have denoted the dipole moments of the $|1\rangle \Leftrightarrow |2\rangle$ and $|2\rangle \Leftrightarrow |3\rangle$ transitions by $\underline{D}_{12}$ and $\underline{D}_{23}$, respectively. The frequencies ω_1, ω_2, and ω_3 are associated with the energies of the electronic states $|1\rangle$, $|2\rangle$, and $|3\rangle$ and the operators $\hat{a}$ ($\hat{a}^\dagger$) and $\hat{b}$ ($\hat{b}^\dagger$) are the annihilation (creation) operators for vibrational quanta in the x and y directions. These operators are related to the position of the ion in the x-y plane through

$$\hat{x} = \Delta x_0(\hat{a} + \hat{a}^\dagger),$$

$$\hat{y} = \Delta y_0(\hat{b} + \hat{b}^\dagger), \tag{6}$$

where $\Delta x_0 = (\hbar/2\nu_a m)^{1/2}$ and $\Delta y_0 = (\hbar/2\nu_b m)^{1/2}$ are the widths of the ground state in the two-dimensional harmonic-oscillator potential in the x and y directions and m is the mass of the ion. If the laser beams are sufficiently far detuned, i.e.,

$$|\Delta_{12}|, |\Delta_{23}| \gg |g_{12}|, |g_{23}|, |\Delta_{12} - \Delta_{23}|, \tag{7}$$

the two ground states $|1\rangle$ and $|3\rangle$ are coupled via a stimulated Raman transition and the excited state $|2\rangle$ can be adiabatically eliminated. In the above inequality we have defined the laser detunings $\Delta_{12} = (\omega_2 - \omega_1) - \omega_{12}$ and $\Delta_{23} = (\omega_2 - \omega_3) - \omega_{23}$ and the dipole coupling constants $g_{12} = \langle 1|\underline{D}_{12}\cdot\underline{e}_{12}|2\rangle E_{12}/\hbar$ and $g_{23} = \langle 3|\underline{D}_{23}\cdot\underline{e}_{23}|2\rangle E_{23}/\hbar$. As described in the Appendix, the adiabatic elimination procedure leads to the Hamiltonian

$$\hat{H} = \hbar\tilde{\omega}_1|1\rangle\langle 1| + \hbar\tilde{\omega}_3|3\rangle\langle 3| + \hbar\nu_a(\hat{a}^\dagger\hat{a}) + \hbar\nu_b(\hat{b}^\dagger\hat{b}) - \hbar g_{13}e^{-i[k_{12}\hat{x} - k_{23}\hat{y} - (\omega_{12}-\omega_{23})t]}\otimes|1\rangle\langle 3| - \hbar g_{13}^* e^{i[k_{12}\hat{x} - k_{23}\hat{y} - (\omega_{12}-\omega_{23})t]}\otimes|3\rangle\langle 1|, \tag{8}$$

where we have dropped the term describing the free energy of the excited state $|2\rangle$ as in the far detuned limit (7) the

excited state is no longer connected to the two ground states. Furthermore, we have defined the Raman coupling constant

$$g_{13}=g_{12}g_{23}^{*}\left(\frac{1}{\Delta_{12}}+\frac{1}{\Delta_{23}}\right) \tag{9}$$

and the energies $\hbar\tilde{\omega}_1$ and $\hbar\tilde{\omega}_3$ of the ground state levels $|1\rangle$ and $|3\rangle$, which are Stark shifted as a result of the adiabatic elimination of the excited state, are

$$\tilde{\omega}_1=\omega_1-\frac{2|g_{12}|^2}{\Delta_{12}},$$

$$\tilde{\omega}_3=\omega_3-\frac{2|g_{23}|^2}{\Delta_{23}}. \tag{10}$$

In order to proceed, we will consider the Raman coupling Hamiltonian (8) in the interaction picture of $\hat{H}_0=\hbar\tilde{\omega}_1|1\rangle\langle 1|+\hbar\tilde{\omega}_3|3\rangle\langle 3|+\hbar\nu_a(\hat{a}^{\dagger}\hat{a})+\hbar\nu_b(\hat{b}^{\dagger}\hat{b})$ and transform to the new Hamiltonian

$$\hat{H}_I=e^{i\hat{H}_0t/\hbar}(\hat{H}-\hat{H}_0)e^{-i\hat{H}_0t/\hbar}. \tag{11}$$

In doing so and replacing the position operators $\hat{x}$ and $\hat{y}$ by Eq. (6) we obtain the interaction Hamiltonian

$$\begin{aligned}\hat{H}_I=&-\hbar g_{13}\exp\left[-\frac{1}{2}(\eta_{12}^2+\eta_{23}^2)\right]|1\rangle\langle 3|\\&\otimes\sum_{m,\mu,n,\nu}\frac{(-i\eta_{12})^{m+\mu}}{m!\mu!}\frac{(i\eta_{23})^{n+\nu}}{n!\nu!}\hat{a}^{\dagger m}a^{\mu}\hat{b}^{\dagger\nu}b^{n}\\&\times\exp\{i(\nu_a[m-\mu]+\nu_b[\nu-n]+\Delta_{13})t\}+\text{H.c.},\end{aligned} \tag{12}$$

where we have defined the Raman detuning

$$\Delta_{13}=\omega_{12}-\omega_{23}-(\tilde{\omega}_3-\tilde{\omega}_1) \tag{13}$$

and the Lamb-Dicke parameters in the x and y directions $\eta_{12}=\Delta x_0k_{12}$ and $\eta_{23}=\Delta y_0k_{23}$. The square of the Lamb-Dicke parameter gives the ratio of the single-photon recoil energy to the energy-level spacing in the harmonic-oscillator potential.

III. SPECIFIC COUPLING SCHEME

In this section we construct a particular configuration of Raman lasers to decouple the electronic and motional dynamics of the trapped ion for suitably chosen initial electronic states. This is done by symmetrically combining two Raman transitions as described below. We then obtain the Hamiltonian (1) in the Lamb-Dicke approximation and in the limit of suitable trap anisotropy for specific sideband detunings of the lasers.

The electronic and motional dynamics can be decoupled in general for the Hamiltonian $\hat{H}_I=\hat{M}\otimes|1\rangle\langle 3|+\hat{M}^{\dagger}\otimes|3\rangle\langle 1|$, where $\hat{M}$ may be any operator that acts on the motional degrees of freedom only. This is done through the addition of another interaction generated by $\hat{H}_I'=\hat{M}\otimes|3\rangle\langle 1|+\hat{M}^{\dagger}\otimes|1\rangle\langle 3|$. Combining both interactions, we have $\hat{H}_I^{\text{tot}}=\hat{H}_I+\hat{H}_I'$, so that the combined Hamiltonian $\hat{H}_I^{\text{tot}}=(\hat{M}+\hat{M}^{\dagger})\otimes(|3\rangle\langle 1|+|1\rangle\langle 3|)$ factorizes. For the case where $\hat{H}_I$ is given by Eq. (12), $\hat{H}_I'$ can be generated by an extra pair of Raman lasers with suitable detunings, propagation directions, and phases. To be more specific, we require a symmetric combination of two Raman transitions, so that

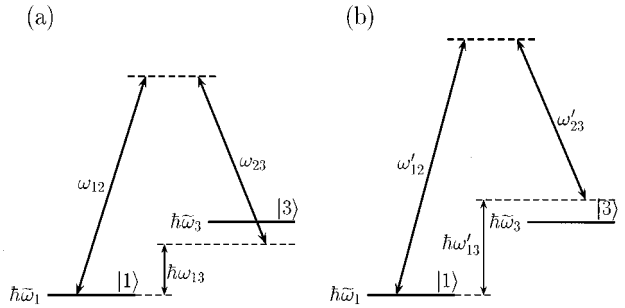

FIG. 2. Schematic diagram of two symmetric Raman transitions that in combination decouple the electronic and motional dynamics of the trapped ion for suitably cosen initial electronic states. In (a), the frequencies ω_{12} and ω_{23} of the two lasers that generate the stimulated Raman transition between the ground state levels $|1\rangle$ and $|3\rangle$ are chosen such that the Raman detuning $\Delta_{13}=\omega_{12}-\omega_{23}-(\tilde{\omega}_3-\tilde{\omega}_1)$ is positive. The coupling lasers are red detuned with respect to the $|1\rangle\Leftrightarrow|3\rangle$ transition. In (b), we show the symmetric Raman transition to (a). The frequencies ω_{12}' and ω_{23}' of the coupling lasers are adjusted so that $\Delta_{13}'=\omega_{12}'-\omega_{23}'-(\tilde{\omega}_3-\tilde{\omega}_1)=-\Delta_{13}$. The coupling beams are blue detuned with respect to the $|1\rangle\Leftrightarrow|3\rangle$ transition. For the two transitions to be symmetric we additionally require the coupling beams in (b) to be counterpropagating with respect to the beams in (a).

$$\Delta_{13}'=-\Delta_{13}, \tag{14}$$

$$\eta_{12}'=-\eta_{12},$$

$$\eta_{23}'=-\eta_{23}, \tag{15}$$

$$g_{13}'=g_{13}^{*}, \tag{16}$$

where all quantities without primes correspond to the first pair of Raman lasers and all primed quantities refer to the second pair. If, for the first pair of lasers, the Raman detuning Δ_{13} is given by Eq. (13), then the first condition (14) requires an appropriate choice of the frequencies ω_{12}' and ω_{23}' for the second pair, so that $\Delta_{13}'=\omega_{12}'-\omega_{23}'-(\tilde{\omega}_3-\tilde{\omega}_1)=-\Delta_{13}$. This is illustrated in Fig. 2. The second condition (15) is satisfied by choosing the second pair of beams to be counterpropagating with respect to the first pair, so that $k_{12}'=-k_{12}$ and $k_{23}'=-k_{23}$, as seen from the definition of the Lamb-Dicke parameters $\eta_{12}=\Delta x_0k_{12}$ and $\eta_{23}=\Delta y_0k_{23}$. Here we have neglected the differences $|k_{12}|-|k_{12}'|$ and $|k_{23}|-|k_{23}'|$ since $|\omega_{12}-\omega_{12}'|\ll\omega_{12},\omega_{12}'$ and $|\omega_{23}-\omega_{23}'|\ll\omega_{23},\omega_{23}'$. This restriction can be lifted if one chooses the second pair of lasers to be not exactly counterpropagating with the first. The third condition (16) requires a suitable choice of laser phases for the two pairs of Raman beams that can be easily read from Eq. (9).

The symmetric combination of the two Raman transitions as specified by Eqs. (14)–(16) then leads to the interaction Hamiltonian

$$\hat{H}_I^{\rm tot} = -\hbar\Bigg\{ g_{13}\exp\Bigg[-\frac{1}{2}(\eta_{12}^2+\eta_{23}^2)\Bigg] \times \sum_{m,\mu,n,\nu} \frac{(-i\eta_{12})^{m+\mu}}{m!\mu!}\frac{(i\eta_{23})^{n+\nu}}{n!\nu!}\hat{a}^{\dagger m}a^{\mu}\hat{b}^{\dagger\nu}b^{n} \times \exp\{i(\nu_a[m-\mu]+\nu_b[\nu-n]+\Delta_{13})t\}+\text{H.c.}\Bigg\} \otimes\{|1\rangle\langle 3|+|3\rangle\langle 1|\}, \tag{17}$$

which factorizes. We now assume the ion to be initially in a direct product of its motional and electronic state with the electronic state prepared as $|+\rangle=(|1\rangle+|3\rangle)/\sqrt{2}$. This superposition state $|+\rangle$ can be prepared from the ground state $|1\rangle$ by applying a resonant $\pi/2$ pulse ($\Delta_{13}=0$) if the ion is confined within the Lamb-Dicke limit, i.e., $\eta_{12},\eta_{23}\ll 1$ [9]. The dynamics generated by Eq. (17) acting on this state factors and leaves the electronic state unchanged. This allows us to reduce the dynamics to that of the motional degrees of freedom only and we write

$$\hat{H}_I^{\rm tot} = -\hbar g_{13}\exp\Bigg[-\frac{1}{2}(\eta_{12}^2+\eta_{23}^2)\Bigg] \times \sum_{m,\mu,n,\nu} \frac{(-i\eta_{12})^{m+\mu}}{m!\mu!}\frac{(i\eta_{23})^{n+\nu}}{n!\nu!}\hat{a}^{\dagger m}a^{\mu}\hat{b}^{\dagger\nu}b^{n} \times \exp\{i(\nu_a[m-\mu]+\nu_b[\nu-n]+\Delta_{13})t\}+\text{H.c.} \tag{18}$$

We now discuss the sideband detunings, which, in the Lamb-Dicke approximation and in the limit of suitable trap anisotropy, lead to the desired interaction (1). In particular, detuning the two pairs of Raman lasers to specific vibrational sidebands allows us to choose specific values for k_a and k_b in Eq. (1). Since we require the two Raman transitions to be symmetric, it is sufficient to consider the first pair of Raman lasers. Therefore, we return to the vibronic Raman coupling Hamiltonian (12). From Eq. (12) it is clear that by fixing the size of the detuning Δ_{13}, i.e., by choosing the frequencies of the two coupling lasers, we can tune to a resonance between specific vibronic levels. As illustrated in Fig. 3, we introduce a virtual level $|c\rangle$ with energy $\hbar\omega_c$ to help visualize the Raman transitions between the ion's vibronic levels. If we set $\omega_{12}=(\omega_c-\tilde{\omega}_1)-k_a\nu_a$ and $\omega_{23}=(\omega_c-\tilde{\omega}_3)-k_b\nu_b$, then with respect to level $|c\rangle$ the first laser is tuned to the k_ath red sideband of the ion's vibration in the x direction, the second laser is tuned to the k_bth red sideband of the vibration in the y direction, and the Raman detuning is

$$\Delta_{13}=k_b\nu_b-k_a\nu_a. \tag{19}$$

This situation is illustrated in Fig. 3 for the specific example $k_a=k_b=1$. Now, if only on-resonant terms in Eq. (12) are retained, we have $m=\mu+k_a$ and $n=\nu+k_b$ and we obtain the Hamiltonian

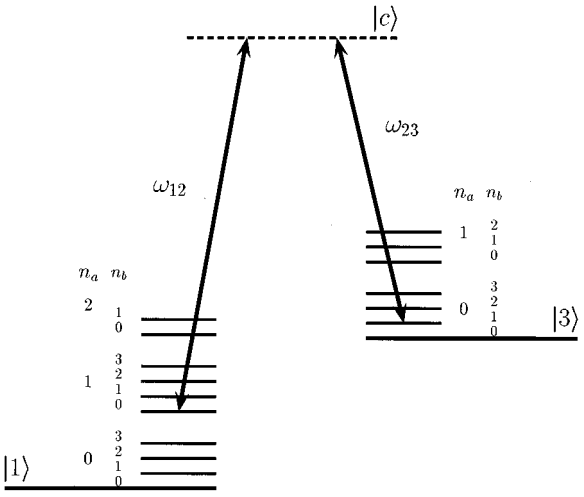

FIG. 3. Schematic diagram of the vibronic energy levels that are connected by the two laser beams that generate the stimulated Raman transition. The two Raman lasers are tuned such that the Raman detuning $\Delta_{13}=k_b\nu_b-k_a\nu_a$, with $k_a=k_b=1$. With respect to the virtual level $|c\rangle$, the laser propagating in the x direction is tuned to the first red sideband of the ion's vibration in the x direction and the laser that propagates in the y direction is tuned to the first red sideband of the ion's vibration in the y direction. This causes a resonant transition between the vibronic states $|n_a-1\rangle_a|n_b\rangle_b|3\rangle\Leftrightarrow|n_a\rangle_a|n_b-1\rangle_b|1\rangle$, where the states $|n_a\rangle_a|n_b\rangle_b$ denote the usual number state basis for the two-dimensional harmonic oscillator and the numbers n_a and n_b give the number of vibrational excitations in the x and y directions, respectively.

$$\hat{H}_I=|1\rangle\langle 3|\otimes\sum_{\mu,\nu}\hbar g(\mu,\nu)\hat{a}^{\dagger k_a}\hat{a}^{\dagger\mu}\hat{a}^{\mu}\hat{b}^{\dagger\nu}\hat{b}^{\nu}\hat{b}^{k_b}+\text{H.c.}, \tag{20}$$

where we have defined the coupling constants

$$g(\mu,\nu)=-g_{13}\exp\Bigg[-\frac{1}{2}(\eta_{12}^2+\eta_{23}^2)\Bigg] \times\frac{(-i\eta_{12})^{2\mu+k_a}}{\mu!(\mu+k_a)!}\frac{(i\eta_{23})^{2\nu+k_b}}{\nu!(\nu+k_b)!}. \tag{21}$$

This is a two-mode generalization of the nonlinear Jaynes-Cummings model introduced by Vogel and de Matos Filho [4]. It is important for the trap frequencies ν_a and ν_b to be noncommensurate to arrive at this result. This becomes clear from Fig. 3. If the trapping potential is isotropic, $\nu_a=\nu_b$ and the energy levels become degenerate. Consequently, the Raman transition Hamiltonian (12) contains on-resonant terms in addition to the ones retained in Eq. (20). In the example $k_a=k_b=1$, this leads to a coupling Hamiltonian $\hat{H}_I \propto[1+\eta^2(\hat{a}^{\dagger}\hat{b}+\hat{a}\hat{b}^{\dagger}-\hat{a}^{\dagger}\hat{a}-\hat{b}^{\dagger}\hat{b})+O(\eta^4)]\otimes|1\rangle\langle 3|+$ H.c., where we have assumed the Lamb-Dicke parameters to be of the same order of magnitude, $\eta_{12}\approx\eta_{23}\approx\eta$. In general, if the frequencies ν_a and ν_b are commensurate, the Raman transition Hamiltonian (12) contains resonances in addition to the ones considered in Eq. (20). As we will show in Sec. IV, in the Lamb-Dicke limit, the coupling constants corresponding to these additional resonances can be greatly reduced by increasing the ratio of the trap frequencies ν_a/ν_b.

The symmetric Raman transition is generated by a second pair of lasers as specified in Eqs. (14)–(16). In particular, we note that Eq. (14) can be satisfied with the choice $\omega'_{12}=(\omega_c-\tilde{\omega}_1)+k_a\nu_a$ and $\omega'_{23}=(\omega_c-\tilde{\omega}_3)+k_b\nu_b$ for the frequencies of the second pair of lasers. With respect to the virtual level $|c\rangle$, these lasers are then detuned by the same amount as the first pair, but to the blue vibrational sidebands rather than the red. Combining both Raman transitions, we obtain the reduced Hamiltonian

$$\hat{H}_I^{\rm tot}=\sum_{\mu,\nu}\hbar g(\mu,\nu)\hat{a}^{\dagger k_a}\hat{a}^{\dagger\mu}\hat{a}^{\mu}\hat{b}^{\dagger\nu}\hat{b}^{k_b}+\text{H.c.} \qquad (22)$$

for the motional dynamics of the trapped ion as discussed above.

In the last step, we now assume the Lamb-Dicke limit, where $\eta_{12},\eta_{23}\ll 1$. In this limit we approximate Eq. (22) by keeping only the lowest-order terms in η_{12} and η_{23}. From Eq. (21) these are the terms $\mu=\nu=0$ and we obtain

$$\hat{H}_I^{\rm tot}=\hbar\{g\hat{a}^{\dagger k_a}\hat{b}^{k_b}+g^*\hat{a}^{k_a}\hat{b}^{\dagger k_b}\}, \qquad (23)$$

where $g=g(0,0)$ is given in Eq. (21). The above Hamiltonian (23) realizes the desired interaction (1) between the two modes a and b of the ion's motion in the x and y directions. We note that the coupling constant g depends on the Lamb-Dicke parameters through the factor $\eta_{12}^{k_a}\eta_{23}^{k_b}$. Consequently, for fixed laser power, i.e., fixed $|g_{12}|$ and $|g_{23}|$, and small Lamb-Dicke parameters, the coupling strength may be very small. One can increase the coupling constant g by increasing the laser power while at the same time maintaining inequality (7). This permits us to ignore the spontaneous emission from the excited state $|2\rangle$ on a time scale

$$T\ll T_{\rm spont}=\left(\frac{|g_{12}|^2}{\Delta_{12}^2}+\frac{|g_{23}|^2}{\Delta_{23}^2}\right)^{-1}\gamma^{-1}, \qquad (24)$$

where γ is the rate of spontaneous decay from level $|2\rangle$ [24]. This is important as the decoupling of the motional and electronic dynamics relies on maintaining the coherence of the electronic degrees of freedom. In Sec. V we will compare the time scales for spontaneous emission and the Raman-generated motional dynamics for the specific case of rotation (2), given the parameters of recent experiments [7].

IV. LIMITATIONS

In this section we further discuss the approximations under which the Hamiltonian (23) gives a valid description of the system dynamics. First, we address the size of the corrections that we have neglected in the Lamb-Dicke approximation. We then show that the coupling constants of the additional resonances in the case of commensurate trap frequencies can be made as small as these corrections for a suitably large ratio of the trap frequencies ν_a/ν_b. Finally, we discuss the limitations imposed on our Hamiltonians from neglecting off-resonant transitions.

A. Lamb-Dicke approximation

From the preceding section it is clear that the Lamb-Dicke limit is an important requirement for us to engineer the desired interaction (23). The Lamb-Dicke approximation led us from Eq. (22) to Eq. (23) under the assumption $\eta_{12},\eta_{23}\ll 1$. We note that both Eqs. (22) and (23) couple the same vibrational states

$$|m\rangle_a|n+k_b\rangle_b\Leftrightarrow|m+k_a\rangle_a|n\rangle_b, \qquad (25)$$

where $|m\rangle_a|n\rangle_b$ denotes the usual number state basis for the two-dimensional harmonic oscillator. Therefore, we do not neglect any additional resonances between states other than the ones given in Eq. (25) by making the Lamb-Dicke approximation.

We define the Lamb-Dicke approximation for suitably small η_{12},η_{23} to be the approximation where all terms in Eq. (22) of order η^2 smaller than the leading term are neglected, i.e.,

$$\frac{|g(\mu,\nu)|}{|g(0,0)|}\leqslant O(\eta^2), \qquad (26)$$

where we have assumed the Lamb-Dicke parameters to be of the same order of magnitude, $\eta_{12}\approx\eta_{23}\approx\eta$.

It is important to note that the orthogonality of the Raman laser beams shown in Fig. 1 is not essential. In fact, the size of the Lamb-Dicke parameters can be reduced by changing the geometry of the lasers and choosing the two Raman beams to be almost counterpropagating. In this situation the wave vectors $\underline{k}_{12}$ and $\underline{k}_{23}$ of the two Raman beams have to be added and the numbers k_{12} and k_{23} in Eq. (8) are then the projections of $\underline{k}=\underline{k}_{12}+\underline{k}_{23}$ onto the x and y axes, respectively.

B. Trap anisotropy

As we have mentioned in Sec. III, even in the case of an anisotropic trap, there are on-resonant terms in addition to the ones included in Eq. (20) when the trap frequencies are commensurate. This is illustrated in Fig. 4, where $\nu_a=5\nu_b$ and again $k_a=k_b=1$. In addition to the $|m-1\rangle_a|n\rangle_b|3\rangle\Leftrightarrow|m\rangle_a|n-1\rangle_b|1\rangle$ transition shown in Fig. 3, the $|m\rangle_a|n-4\rangle_b|3\rangle\Leftrightarrow|m\rangle_a|n\rangle_b|1\rangle$ transition is resonantly coupled as in Fig. 4. In the following we show that in the Lamb-Dicke limit, the coupling constants $\tilde{g}$, corresponding to these additional resonances, satisfy

$$\frac{|\tilde{g}|}{|g(0,0)|}\leqslant O(\eta^2) \qquad (27)$$

if the ratio of the trap frequencies is chosen large enough. These additional terms can thus be neglected in the Lamb-Dicke approximation.

We start by deriving the resonances that occur if the two trap frequencies ν_a and ν_b are multiples of each other. Without loss of generality we choose

$$\nu_a=l\nu_b, \qquad (28)$$

where l is a positive integer number. In deriving the interaction (23) the laser frequencies were chosen to give the detunings $\Delta_{13}=k_b\nu_b-k_a\nu_a$ and $\Delta'_{13}=k_a\nu_a-k_b\nu_b$ for the two pairs of coupling beams, respectively. We will explicitly consider only the first of these two cases, i.e.,

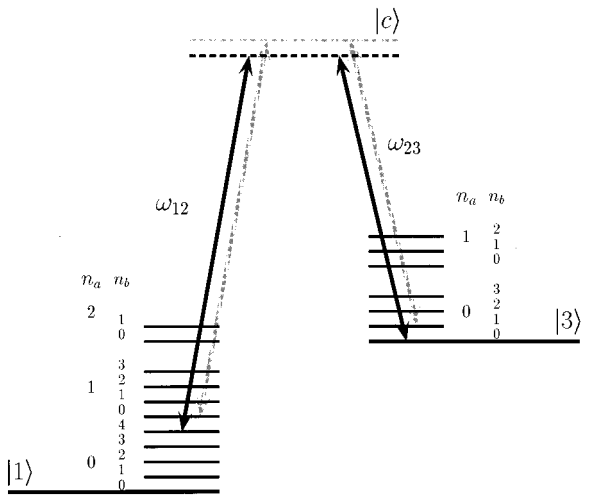

FIG. 4. Vibronic energy-level diagram for the case of the two trap frequencies ν_a and ν_b being multiples of each other, $\nu_a=5\nu_b$. As in Fig. 3 the two Raman lasers are tuned such that the Raman detuning $\Delta_{13}=k_b\nu_b-k_a\nu_a$, with $k_a=k_b=1$. In addition to the desired resonant transition $|n_a-1\rangle_a|n_b\rangle_b|3\rangle\Leftrightarrow|n_a\rangle_a|n_b-1\rangle_b|1\rangle$, shown in gray, the $|n_a\rangle_a|n_b-4\rangle_b|3\rangle\Leftrightarrow|n_a\rangle_a|n_b\rangle_b|1\rangle$ transition is resonantly coupled, as shown in black. In the Lamb-Dicke limit, the coupling constant corresponding to this additional resonance can be reduced to the size of the corrections to the Lamb-Dicke approximation for the desired resonance by increasing the ratio of the trap frequencies ν_a/ν_b.

$\Delta_{13}=k_b\nu_b-k_a\nu_a$, since the second follows analogously by interchanging the operators $\hat{a}\Leftrightarrow\hat{a}^\dagger$ and $\hat{b}\Leftrightarrow\hat{b}^\dagger$ and leads to the same limits for the trap ratio $l=\nu_a/\nu_b$. Now, with Eq. (28), the resonance condition in Eq. (12) becomes

$$-l(\mu-m)-(n-\nu)-lk_a+k_b=0, \tag{29}$$

where all numbers are positive integers. In order to simplify the discussion we categorize the resonances by introducing an integer number N and rewrite Eq. (29) so that

$$\mu-m=-k_a+N,$$
$$\nu-n=-k_b+lN. \tag{30}$$

Following this categorization, we divide the resonances determined by Eq. (29) into the three cases (i) $N=0$, (ii) N positive, and (iii) N negative. We subdivide case (ii) further into (ii a 1) $0<N\leqslant k_a$, $0<Nl\leqslant k_b$ and (ii a 2) $0<N\leqslant k_a$, $Nl>k_b$, and (ii b 1) $N>k_a$, $0<Nl\leqslant k_b$ and (ii b 2) $N>k_a$, $Nl>k_b$. Below we will examine cases (i) and (ii a 2) in detail as the latter case contains resonances with the largest contribution besides the required resonance at $N=0$. We have examined the other cases and will not repeat their analysis except to note that they all give rise to leading-order corrections of order higher than those found in case (ii a 2) in η. Thus, to obtain the desired Hamiltonian (23), the resonances in case (ii a 2) will impose the most stringent condition on the size of the trap ratio $l=\nu_a/\nu_b$. Throughout this discussion we will consider only the lowest-order terms in the Lamb-Dicke parameters since we have already addressed the size of the corrections to the Lamb-Dicke approximation in the above.

In case (i) we have $N=0$, so that from the resonance condition in Eq. (30) we obtain $\mu-m=-k_a$ and $\nu-n=-k_b$. This is the case that leads us to the desired interaction (23), which we have discussed in Sec. III.

We now consider case (ii a 2). Here we have $0<N\leqslant k_a$ and $Nl>k_b$, so that from Eq. (30) we obtain

$$m=\mu+k_a-N\geqslant\mu, \tag{31}$$
$$\nu=n+lN-k_b>n.$$

Inserting these identities into Eq. (12) and keeping only the lowest-order terms in the Lamb-Dicke approximation, i.e., $\mu=n=0$, we obtain

$$\hat{H}_I=\hbar\tilde{g}\hat{a}^{\dagger k_a-N}\hat{b}^{\dagger lN-k_b}|1\rangle\langle 3|+\text{H.c.}, \tag{32}$$

where we have defined the coupling constant

$$\tilde{g}=-g_{13}\exp\left[-\frac{1}{2}(\eta_{12}^2+\eta_{23}^2)\right]\frac{(-i\eta_{12})^{k_a-N}}{(k_a-N)!}\frac{(i\eta_{23})^{lN-k_b}}{(lN-k_b)!}. \tag{33}$$

We require the coupling constants of the above resonances (31) to be smaller than or equal to the coupling constants of the terms that we have neglected in the Lamb-Dicke limit (27). Therefore, we have the condition

$$\frac{|\tilde{g}|}{|g(0,0)|}=\frac{k_a!}{(k_a-N)!}\frac{k_b!}{(lN-k_b)!}\frac{(\eta_{23})^{lN-2k_b}}{(\eta_{12})^N}\leqslant\eta^2, \tag{34}$$

where again we assume both Lamb-Dicke parameters to be of the same order of magnitude, $\eta_{12}\approx\eta_{23}\approx\eta$. In order to derive a limit for the trap ratio l from the above expression, we consider the factor containing the Lamb-Dicke parameters and the one containing the factorials separately. If $\eta_{12}\approx\eta_{23}\approx\eta$, we have

$$\frac{(\eta_{23})^{lN-2k_b}}{(\eta_{12})^N}\approx\eta^{N(l-1)-2k_b}\leqslant\eta^2, \tag{35}$$

which is satisfied if $N(l-1)-2k_b\geqslant 2$. Since this condition has to hold for all N in the range $0<N\leqslant k_a$, this leads to the requirement

$$l\geqslant 2k_b+3 \tag{36}$$

for the trap ratio l. Next we consider the term including the factorials. We require this term to be smaller than or equal to unity as under the above condition (36) the factor containing the Lamb-Dicke parameters already satisfies Eq. (35). We have

$$\frac{k_a!}{(k_a-N)!}\frac{k_b!}{(lN-k_b)!}\leqslant\frac{k_a!k_b!}{(lN-k_b)!}\leqslant\frac{(k_a+k_b)!}{(lN-k_b)!}, \tag{37}$$

where in the first inequality we made use of the fact that for the resonances we are discussing here $0<N\leqslant k_a$ and the second inequality holds since $(k_a+k_b)!\geqslant k_a!k_b!$ for all positive integers k_a and k_b. From the above inequality (37) the factor containing the Lamb-Dicke parameters is smaller than

or equal to unity if $(lN-k_b)! \geqslant (k_a+k_b)!$ and since this has to be satisfied for all N in the range $0<N\leqslant k_a$ we require

$$l \geqslant 2k_b + k_a . \tag{38}$$

Depending on the interaction that we want to generate, i.e., depending on the number k_a, the inequality (36) or (38) will impose the stronger limit on the trap anisotropy. For the two examples given in Eqs. (2) and (3), we have $k_a=k_b=1$ and $k_a=3$, $k_b=1$, respectively. Therefore, in order to generate the linear coupling Hamiltonian (2) we require the trap ratio $l=\nu_a/\nu_b \geqslant 5$ (36). For the cubic interaction (3) a trap ratio of $l=\nu_a/\nu_b \geqslant 5$ is needed from Eq. (38). For the remaining cases (ii a 1), (ii b 1), (ii b 2), and (iii) a similar analysis shows that the requirements (36) and (38) are sufficient to limit the strength of these resonances to Eq. (27).

Although in the above discussion we have explicitly assumed the two trap frequencies ν_a and ν_b to be multiples of each other, the limits (36) and (38) also hold for commensurate trap frequencies. In this case the trap ratio is a rational number, i.e., $l=p/q$, where p and q are positive integers. Since in the resonance condition (30) all numbers need to be integers, the number N that categorizes the resonances can only take on multiple values of q, so that $lN=pN/q$ is an integer. As we have discussed all integer values of N, any trap ratio $l=p/q$ that satisfies inequalities (36) and (38) suffices for the unwanted resonances to satisfy Eq. (27). Hence, for given values of k_a and k_b, the coupling constants of all additional resonances due to energy-level degeneracies in the case of commensurate trap frequencies are at least a factor of η^2 smaller than the coupling constant of the desired resonance (23) if the trap ratio is chosen large enough according to the limits in Eqs. (36) and (38).

C. Off-resonant terms

As pointed out by Gardiner *et al.* [25], dropping all off-resonant terms in going from Eq. (18) to Eq. (23) imposes a limit on the time T for which the Hamiltonian (23) is a valid approximation. This limit can be calculated in second-order perturbation theory to be $TV^2/\Delta \ll 1$, where V is the effective coupling to the nearest off-resonant transition in Eq. (18) and Δ is the corresponding detuning. If $|M\rangle_a|N\rangle_b$ is a characteristic state that represents the highest-energy state that we allow to be acted upon, the transitions

$$\begin{aligned} |M-k_a+1\rangle_a|N\rangle_b &\Leftrightarrow |M\rangle_a|N-k_b\rangle_b , \\ |M-k_a\rangle_a|N\rangle_b &\Leftrightarrow |M\rangle_a|N-k_b+1\rangle_b \end{aligned} \tag{39}$$

are the strongest coupled off-resonant terms. For these two transitions the limit becomes

$$\begin{aligned} T|g(0,0)|^2 \frac{M!N!}{(M-k_a+1)!(N-k_b)!}\left(\frac{k_a}{\eta_{12}}\right)^2 &\ll \nu_a , \\ T|g(0,0)|^2 \frac{M!N!}{(M-k_a)!(N-k_b+1)!}\left(\frac{k_b}{\eta_{23}}\right)^2 &\ll \nu_b , \end{aligned} \tag{40}$$

where we have assumed the Lamb-Dicke limit to calculate the coupling V between the states (39). We will further investigate the significance of the limitations discussed here in the following section where we concentrate on the linear coupling Hamiltonian $\hat{H}_I^{(1)}$ given in Eq. (2).

V. ENGINEERING ROTATION

In the following we use the above formalism to target the linear coupling Hamiltonian $\hat{H}_I^{(1)}$ given in Eq. (2) and show how this generates a rotation of the two-dimensional quantum motional state of the ion. We then examine the validity of the approximations discussed in the preceding section through a numerical analysis of this specific example.

The linear coupling $\hat{H}_I^{(1)}$ is obtained from the symmetrically combined two-mode Raman Hamiltonian (18) through the particular choice $\Delta_{13}=\nu_b-\nu_a$ for the Raman detuning and adjusting the relative phase of the lasers such that the Raman coupling constant $g_{13}=i|g_{13}|$ is purely imaginary. This leads to the Hamiltonian

$$\begin{aligned} \hat{H}_I^{\mathrm{tot}} = &-i\hbar|g_{13}|\exp\left[-\frac{1}{2}(\eta_{12}^2+\eta_{23}^2)\right] \\ &\times \sum_{m,\mu,n,\nu} \frac{(-i\eta_{12})^{m+\mu}}{m!\mu!}\frac{(i\eta_{23})^{n+\nu}}{n!\nu!}\hat{a}^{\dagger m}a^{\mu}\hat{b}^{\dagger \nu}b^{n} \\ &\times \exp\{i(\nu_a[m-\mu-1]+\nu_b[\nu+1-n]+\Delta_{13})t\}+\mathrm{H.c.}, \end{aligned} \tag{41}$$

which, in the limits discussed in Sec. IV, results in the linear coupling $\hat{H}_I^{(1)}$. The coupling constant g in Eq. (2) is then given by $g=-|g(0,0)|$. The Hamiltonian $\hat{H}_I^{(1)}$ effects a rotation of the two-dimensional quantum motional state of the ion about the center of the trap. This can be seen by examining the action of the Hamiltonian $\hat{H}_I^{(1)}$ on the operators $\hat{a}$ and $\hat{b}$. Using the Baker-Campbell-Hausdorff theorem, we have

$$\begin{aligned} \hat{a}_\theta &= \hat{U}^{(1)}\hat{a}\hat{U}^{(1)^\dagger} = \hat{a}\cos\theta - \hat{b}\sin\theta, \\ \hat{b}_\theta &= \hat{U}^{(1)}\hat{b}\hat{U}^{(1)^\dagger} = \hat{a}\sin\theta + \hat{b}\cos\theta, \end{aligned} \tag{42}$$

where the angle $\theta=gt$ and $\hat{U}^{(1)}$ is the unitary transformation generated by the Hamiltonian $\hat{H}_I^{(1)}$, i.e.,

$$\hat{U}^{(1)} = e^{i\hat{H}_I^{(1)}t/\hbar}. \tag{43}$$

From Eq. (6) it is clear that the transformation in Eq. (42) corresponds to a rotation of the rescaled coordinate system $\tilde{x}=x/\Delta x_0$ and $\tilde{y}=y/\Delta y_0$ through an angle $\theta=gt$, so that in the rotated coordinate system we have

$$\begin{aligned} \tilde{x}_\theta &= \tilde{x}\cos\theta - \tilde{y}\sin\theta, \\ \tilde{y}_\theta &= \tilde{x}\sin\theta + \tilde{y}\cos\theta. \end{aligned} \tag{44}$$

Now an arbitrary pure or mixed motional state of the ion is characterized by a density operator $\hat{\rho}$, which can be written as

$$\hat{\rho}=\sum_{m,n,\mu,\nu}\rho_{m,n}^{\mu,\nu}|m\rangle_a|n\rangle_b\langle\mu|_a\langle\nu|_b$$

$$=\sum_{m,n,\mu,\nu}\rho_{m,n}^{\mu,\nu}\frac{\hat{a}^{\dagger m}\hat{b}^{\dagger n}}{\sqrt{m!n!}}|0\rangle_a|0\rangle_b\langle 0|_a\langle 0|_b\frac{\hat{a}^{\mu}\hat{b}^{\nu}}{\sqrt{\mu!\nu!}}. \quad (45)$$

The time evolution of this state under the action of the Hamiltonian $\hat{H}_I^{(1)}$ is then given by

$$\hat{\rho}(t)=\hat{U}^{(1)}\hat{\rho}\hat{U}^{(1)\dagger}$$

$$=\sum_{m,n,\mu,\nu}\rho_{m,n}^{\mu,\nu}\frac{\hat{a}_\theta^{\dagger m}\hat{b}_\theta^{\dagger n}}{\sqrt{m!n!}}|0\rangle_a|0\rangle_b\langle 0|_a\langle 0|_b\frac{\hat{a}_\theta^{\mu}\hat{b}_\theta^{\nu}}{\sqrt{\mu!\nu!}}$$

$$=\sum_{m,n,\mu,\nu}\rho_{m,n}^{\mu,\nu}|m\rangle_a^\theta|n\rangle_b^\theta\langle\mu|_a^\theta\langle\nu|_b^\theta, \quad (46)$$

where we have used Eq. (42) and $|m\rangle_a^\theta|n\rangle_b^\theta$ is the number state basis for the two-dimensional harmonic oscillator, but now in the rotated coordinates $\tilde{x}_\theta$ and $\tilde{y}_\theta$ as given in Eq. (44). Therefore, the motional state of the ion given by $\hat{\rho}(t)$ is identical to $\hat{\rho}$, but rotated through an angle $\theta=gt$. In particular, this is accomplished without prior knowledge of the motional state $\hat{\rho}$.

Having convinced ourselves that the linear coupling Hamiltonian $\hat{H}_I^{(1)}$ does rotate an arbitrary motional state of the ion, we now examine the validity of the approximations discussed in Sec. IV for this specific example of the general coupling Hamiltonian (23). We consider a state rotation through the angle $\theta=\pi/2$, so that $T_{\rm rot}=\pi/2g$ is the required time to rotate the state. For this case, the limitations due to off-resonant terms (Sec. IV C) as given in Eq. (40) take the form

$$\frac{\pi}{2}N_{\max}\ll\frac{\nu_b}{|g_{13}|} \quad (47)$$

in the limit of small $\eta_{12}\approx\eta_{23}\approx\eta$, where we have assumed ν_b to be the smaller of the two trap frequencies. Here $N_{\max}=\max(N,M)$ in Eq. (40). From Eq. (47) it is clear that the ratio of the lower trap frequency over the Raman coupling constant

$$\gamma=\nu_b/|g_{13}| \quad (48)$$

determines the significance of off-resonant terms in the system dynamics.

From our discussion of the significance of additional on-resonant terms (Sec. IV B) we require a trap ratio $l=\nu_a/\nu_b\geq 5$ for the linear coupler where $k_a=k_b=1$ [Eq. (36)]. The estimates used to determine this minimal trap ratio essentially compare the coupling strengths of the different terms appearing in the Hamiltonian (41) with no reference to the actual state on which it acts. Although this method of estimation is used in the literature, it can serve only as a rough guide. A more rigorous measure of how the unitary time evolution $\hat{U}_{\rm tot}^{(1)}$, generated by the symmetrically combined two-mode Raman Hamiltonian (41), deviates from the desired unitary evolution $\hat{U}^{(1)}$, generated by the linear coupling Hamiltonian (2), can be quite complicated. A fully rigorous state-independent measure of the difference between two unitary operators can be constructed [26], but we will not consider this here. In order to examine the validity of the approximations discussed in Sec. IV we adopt the overlap

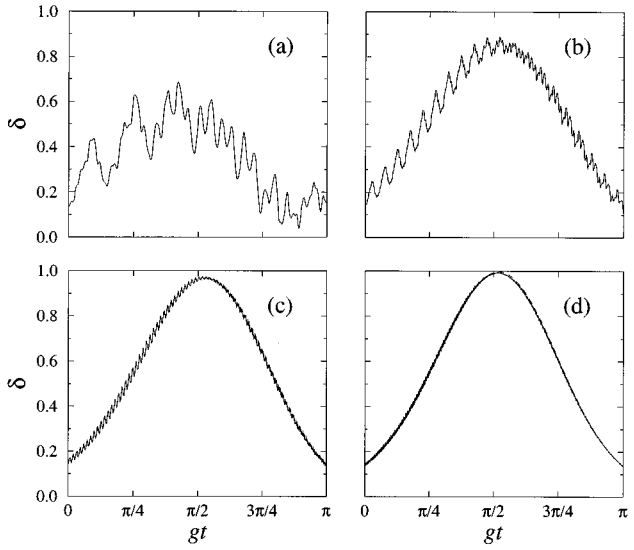

FIG. 5. Results from our numerical analysis of the deviation of the unitary evolution generated by the symmetrically combined Raman Hamiltonian tuned for rotation from the desired state rotation. We plot the overlap $\delta=|\langle\Psi_{\rm tot}|\Psi\rangle|$, between the state $|\Psi_{\rm tot}\rangle$, resulting from the Raman Hamiltonian tuned for rotation, and the desired state $|\Psi\rangle=|-\alpha\rangle_a\otimes|\alpha\rangle_b$, resulting from a rotation of the initial state $|\Psi_0\rangle=|\alpha\rangle_a\otimes|\alpha\rangle_b$, through the angle $\theta=\pi/2$. We have chosen $\alpha=1$. Graphs (a)–(d) show the dependence of the time evolution of δ on the parameter γ, which takes on the values $\gamma=22/2^n$, where $n=3,\ldots,0$ in unit steps.

$$\delta\equiv|\langle\Psi_{\rm tot}|\Psi\rangle| \quad (49)$$

as a measure of the deviation between the two unitary evolutions $\hat{U}_{\rm tot}^{(1)}$ and $\hat{U}^{(1)}$ for an initially pure quantum state $|\Psi_0\rangle$. Here the state

$$|\Psi_{\rm tot}\rangle=\hat{U}_{\rm tot}^{(1)}|\Psi_0\rangle \quad (50)$$

gives the unitary evolution of the initial state $|\Psi_0\rangle$ under the action of the symmetrically combined Raman Hamiltonian (41) and the state

$$|\Psi\rangle=\hat{U}^{(1)}|\Psi_0\rangle \quad (51)$$

gives the desired evolution of the initial state under the action of the linear coupling Hamiltonian (2). This cannot be calculated analytically. To go beyond the analytics we numerically compute the unitary evolution (50), including the higher on-resonant and off-resonant terms, on the initial pure state $|\Psi_0\rangle=|\alpha\rangle_a\otimes|\alpha\rangle_b$, where $|\alpha\rangle_a$ and $|\alpha\rangle_a$ are coherent states in the vibrational modes a and b, respectively. In this case the desired state (51), rotated through $\theta=\pi/2$, is given by $|\Psi\rangle=|-\alpha\rangle_a\otimes|\alpha\rangle_b$. The results of our numerical analysis are shown in Fig. 5. There we plot the overlap δ as a function of the scaled time gt, for different values of the parameter γ, given by Eq. (48) and a coherent state amplitude $\alpha=1$. Before we discuss our results, we note the fol-

lowing on our choice of parameters. In Figs. 5(a)–5(d), γ takes on the values $\gamma=22/2^n$, where $n=3,\ldots,0$ in unit steps, and the Raman coupling constant g_{13} is kept constant. For simplicity, we assume the geometry of the laser excitation to be arranged so that the Lamb-Dicke parameters $\eta_{12}=\Delta x_0 k_{12}$ and $\eta_{23}=\Delta y_0 k_{23}$ are equal. Here it is important to note that the values of the Lamb-Dicke parameters η_{12} and η_{23} depend on the size of the trap frequencies ν_a and ν_b through $\Delta x_0=(\hbar/2\nu_a m)^{1/2}$ and $\Delta y_0=(\hbar/2\nu_b m)^{1/2}$. Therefore, the size of the Lamb-Dicke parameters depends on γ and varies from Fig. 5(a) to 5(d). To incorporate this dependence in our numerical analysis we set $\gamma\eta_{12}^2=\gamma\eta_{23}^2=0.88$, which gives $\eta_{12}=\eta_{23}=0.2$, when $\gamma=22$. These are values for the Lamb-Dicke parameters and the ratio γ that have been demonstrated in cold ion experiments [7–10]. Following our discussion of the trap anisotropy, we choose the trap ratio $l=\nu_a/\nu_b=5$. Our numerical analysis was performed in a finite (truncated) number state basis ($|0\rangle_a|0\rangle_b\cdots|8\rangle_a|8\rangle_b$) with a cutoff chosen such that an increase of this cutoff does not significantly alter the result of our integration. Figure 5(a) shows the time evolution of the overlap δ for the lowest value of γ. Here the off-resonant terms in Eq. (41) cause strong modulations in δ. For higher values of γ these modulations become much less pronounced as the off-resonant terms contribute less on these time scales [Figs. 5(b)–5(d)]. The time evolution of δ for the highest value of γ is shown with the solid line in Fig. 5(d). The plot reaches a maximum of $\delta\approx 0.99$ at $gt\approx 1.02\times\pi/2$. It shows almost no deviation from the dashed line in Fig. 5(d), which is a numerical integration of the system dynamics where we include only the desired resonances in the Hamiltonian as in Eq. (22). The numerical analysis shows that for low system excitation the Hamiltonian $\hat{H}_I^{(1)}$ can be engineered with high accuracy within present ion traps. The investigation of the system dynamics for higher energies becomes computationally very expensive. To achieve the same accuracy as obtained for $\alpha=1$ for higher values of α, the number state basis must be greatly enlarged.

In the above, we neglected decoherence. From our final comments in Sec. III, using the experimental parameters [7] for $^9Be^+$ with $\gamma/2\pi=19$ MHz, $g_{13}/2\pi=500$ kHz, $\Delta_{12}/2\pi=\Delta_{23}/2\pi=12$ GHz, and $\eta_{12}=\eta_{23}=0.2$, we find $T_{\text{spont}}\approx 200\ \mu$s. This is to be compared with the time to rotate the motional state through the angle $\theta=\pi/2$, $T_{\text{rot}}\approx 12\ \mu$s. This confirms our initial assumption that decoherence through spontaneous emission can be neglected for this process. However, this may not be the case when engineering higher-order interactions. One can shorten the interaction time by increasing the laser power while maintaining inequality (7) by increasing the detunings Δ_{12} and Δ_{23}. The fundamental limit is then given by the detunings that one can realize and the accessible laser power.

VI. CONCLUSION

In this work we showed how one can engineer a class of Hamiltonians for the motional dynamics of an ultracold ion in a harmonic trap. The process uses a stimulated Raman transition in a Λ configuration with the two lasers propagating along the x and y directions. To decouple the internal electronic dynamics from the external motional dynamics we constructed a Hamiltonian in which these evolutions factored. This was done through the addition of a second pair of lasers that generated the symmetric counterpart to the Hamiltonian generated by the first pair of lasers. By preparing the electronic states in a particular superposition, the internal and external dynamics completely separated and we could treat the motional dynamics alone. In the Lamb-Dicke limit and with suitable sideband detunings, we could ''target'' a particular term to be of leading order in the Hamiltonian. However, we found that in addition to the term we wanted to dominate, other, higher on-resonant terms appeared. We could manipulate the strengths of the couplings to these unwanted terms by altering the trap frequency ratio and found that we could neglect these unwanted terms in the Lamb-Dicke approximation for large enough trap anisotropies. Finally, we did a numerical evaluation of the full Hamiltonian as a check on the analytical estimates. Although we have primarily concentrated on the linear rotation Hamiltonian (2), higher-order dynamics can be generated, i.e., $\hat{H}_I^{(3)}$ given by Eq. (3). The nonlinear Hamiltonian $\hat{H}_I^{(3)}$ has been much studied in the quantum optical literature as a model of nonlinearly coupled field modes [21]. We know from this work that such Hamiltonians generate a rich nonlinear dynamical structure reflecting the strong mode entanglement characteristic of those couplings. Their optical realization is difficult, but may well be more straightforward in trapped ion dynamics, as resonances can then be used to isolate chosen nonlinearities.

Finally, we note the recent publication of two papers [27] that examine types of nonlinear interaction Hamiltonians in the motion of trapped ions that are closely related to the work presented here.

ACKNOWLEDGMENTS

This work was supported in part by the United Kingdom Engineering and Physical Sciences Research Council and the European Community. J.S. is supported by the German Academic Exchange Service (DAAD-Doktorandenstipendium aus Mitteln des zweiten Hochschulsonderprogramms). We thank Dr. S.-C. Gou for helpful discussions and S. Schneider for her helpful comments on the manuscript.

APPENDIX

In this appendix we derive the effective Hamiltonian given in Eq. (8), which follows from the adiabatic elimination of the excited level $|2\rangle$ and describes the Raman coupling between the two ground-state levels $|1\rangle$ and $|3\rangle$. After performing the rotating-wave approximation, the Hamiltonian in Eq. (5) becomes

$$\begin{aligned}\hat{H}=&\hbar\omega_1|1\rangle\langle 1|+\hbar\omega_2|2\rangle\langle 2|+\hbar\omega_3|3\rangle\langle 3|+\hbar\nu_a(\hat{a}^\dagger\hat{a})\\&+\hbar\nu_b(\hat{b}^\dagger\hat{b})-|1\rangle\langle 2|\otimes\hbar g_{12}e^{-i(k_{12}\hat{x}-\omega_{12}t)}\\&-|2\rangle\langle 1|\otimes\hbar g_{12}^* e^{i(k_{12}\hat{x}-\omega_{12}t)}-|3\rangle\langle 2|\otimes\hbar g_{23}\\&\times e^{-i(k_{23}\hat{y}-\omega_{23}t)}-|2\rangle\langle 3|\otimes\hbar g_{23}^* e^{i(k_{23}\hat{y}-\omega_{23}t)},\end{aligned}\tag{A1}$$

where we have defined the dipole coupling constants $g_{12}=\langle 1|\underline{D}_{12}\cdot\underline{e}_{12}|2\rangle E_{12}/\hbar$ and $g_{23}=\langle 3|\underline{D}_{23}\cdot\underline{e}_{23}|2\rangle E_{23}/\hbar$.

In order to compare the time scales of the transitions induced by the two laser beams we consider the Heisenberg equations of motion for the transition operators $\hat{\sigma}_{12}\equiv|1\rangle\langle 2|$ and $\hat{\sigma}_{13}\equiv|1\rangle\langle 3|$,

$$i\frac{d}{dt}\hat{\bar{\sigma}}_{12}=(\omega_2-\omega_1)\hat{\bar{\sigma}}_{12}-g_{12}^{*}e^{i(k_{12}\hat{\bar{x}}-\omega_{12}t)}(\hat{\bar{\sigma}}_{11}-\hat{\bar{\sigma}}_{22})-g_{23}^{*}e^{i(k_{23}\hat{\bar{y}}-\omega_{23}t)}\hat{\bar{\sigma}}_{13},$$

$$i\frac{d}{dt}\hat{\bar{\sigma}}_{13}=(\omega_3-\omega_1)\hat{\bar{\sigma}}_{13}-g_{23}e^{-i(k_{23}\hat{\bar{y}}-\omega_{23}t)}\hat{\bar{\sigma}}_{12}+g_{12}^{*}e^{i(k_{12}\hat{\bar{x}}-\omega_{12}t)}\hat{\bar{\sigma}}_{23}. \tag{A2}$$

Here all operators (denoted by overbars) are taken in the Heisenberg picture, i.e., $\hat{\bar{\sigma}}_{12}=\hat{U}(t)\hat{\sigma}_{12}\hat{U}^{\dagger}(t)$, where $\hat{U}(T)=\hat{T}\exp\{i[\int^{t}\hat{H}(t')dt'/\hbar]\}$ is the time-ordered evolution operator. Using the transformation

$$\hat{\bar{\sigma}}_{12}=e^{-i\omega_{12}t}\hat{\tilde{\sigma}}_{12},$$

$$\hat{\bar{\sigma}}_{23}=e^{i\omega_{23}t}\hat{\tilde{\sigma}}_{23},$$

$$\hat{\bar{\sigma}}_{13}=\hat{\bar{\sigma}}_{12}\hat{\bar{\sigma}}_{23}=e^{-i(\omega_{12}-\omega_{23})t}\hat{\bar{\sigma}}_{13} \tag{A3}$$

to remove the explicit time dependences from Eq. (A2) we have

$$i\frac{d}{dt}\hat{\tilde{\sigma}}_{12}=\Delta_{12}\hat{\tilde{\sigma}}_{12}-g_{12}^{*}e^{ik_{12}\hat{\bar{x}}}(\hat{\bar{\sigma}}_{11}-\hat{\bar{\sigma}}_{22})-g_{23}^{*}e^{ik_{23}\hat{\bar{y}}}\hat{\tilde{\sigma}}_{13},$$

$$i\frac{d}{dt}\hat{\tilde{\sigma}}_{13}=(\Delta_{12}-\Delta_{23})\hat{\tilde{\sigma}}_{13}-g_{23}e^{-ik_{23}\hat{\bar{y}}}\hat{\tilde{\sigma}}_{12}+g_{12}^{*}e^{ik_{12}\hat{\bar{x}}}\hat{\tilde{\sigma}}_{23}. \tag{A4}$$

Under the assumption of large detunings, as given in Eq. (7), we obtain the adiabatic solution for $\hat{\tilde{\sigma}}_{12}$ by setting $d\hat{\tilde{\sigma}}_{12}/dt\equiv 0$ [28], so that after restoring the rapidly oscillating time dependence, we obtain

$$\hat{\bar{\sigma}}_{12}=\frac{1}{\Delta_{12}}\{g_{12}^{*}e^{i(k_{12}\hat{\bar{x}}-\omega_{12}t)}(\hat{\bar{\sigma}}_{11}-\hat{\bar{\sigma}}_{22})+g_{23}^{*}e^{i(k_{23}\hat{\bar{y}}-\omega_{23}t)}\hat{\bar{\sigma}}_{13}\}. \tag{A5}$$

For the $|2\rangle\Leftrightarrow|3\rangle$ transition we find in an analogous manner

$$\hat{\bar{\sigma}}_{32}=\frac{1}{\Delta_{23}}\{g_{23}^{*}e^{i(k_{23}\hat{\bar{y}}-\omega_{23}t)}(\hat{\bar{\sigma}}_{33}-\hat{\bar{\sigma}}_{22})+g_{12}^{*}e^{i(k_{12}\hat{\bar{x}}-\omega_{12}t)}\hat{\bar{\sigma}}_{31}\}. \tag{A6}$$

Upon inserting these adiabatic solutions for $\hat{\bar{\sigma}}_{12}$ and $\hat{\bar{\sigma}}_{32}$ into Eq. (A1), we have

$$\hat{H}=\hbar\tilde{\omega}_1|1\rangle\langle 1|+\hbar\tilde{\omega}_3|3\rangle\langle 3|+\hbar\nu_a(\hat{a}^{\dagger}\hat{a})+\hbar\nu_b(\hat{b}^{\dagger}\hat{b})-\hbar g_{13}e^{-i[k_{12}\hat{x}-k_{23}\hat{y}-(\omega_{12}-\omega_{23})t]}\otimes|1\rangle\langle 3|-\hbar g_{13}^{*}e^{i[k_{12}\hat{x}-k_{23}\hat{y}-(\omega_{12}-\omega_{23})t]}\otimes|3\rangle\langle 1|, \tag{A7}$$

where we have dropped the term describing the free energy of the excited state $|2\rangle$ since in this adiabatic approximation it is no longer connected to the two ground states. Furthermore, we have defined the Raman coupling constant as given in Eq. (9) and the energies $\hbar\tilde{\omega}_1$ and $\hbar\tilde{\omega}_3$ (10) of the ground-state levels $|1\rangle$ and $|3\rangle$, which are Stark shifted as a result of the adiabatic elimination of the excited state.

[1] F. Diedrich, J. C. Bergquist, W. M. Itano, and D. J. Wineland, Phys. Rev. Lett. **62**, 403 (1989); C. Monroe, D. M. Meekhof, B. E. King, S. R. Jefferts, W. M. Itano, and D. J. Wineland, *ibid.* **75**, 4011 (1995).

[2] C. A. Blockley, D. F. Walls, and H. Risken, Europhys. Lett. **17**, 509 (1992); C. A. Blockley and D. F. Walls, Phys. Rev. A **47**, 2115 (1993).

[3] J. I. Cirac, R. Blatt, A. S. Parkins, and P. Zoller, Phys. Rev. Lett. **70**, 762 (1993); J. I. Cirac, A. S. Parkins, R. Blatt, and P. Zoller, *ibid.* **70**, 556 (1993).

[4] W. Vogel and R. L. de Matos Filho, Phys. Rev. A **52**, 4214 (1995).

[5] R. L. de Matos Filho and W. Vogel, Phys. Rev. Lett. **76**, 608 (1996).

[6] R. L. de Matos Filho and W. Vogel, Phys. Rev. A **54**, 4560 (1996).

[7] D. M. Meekhof, C. Monroe, B. E. King, W. M. Itano, and D. J. Wineland, Phys. Rev. Lett. **76**, 1796 (1996).

[8] D. Leibfried, D. M. Meekhof, B. E. King, C. Monroe, W. M. Itano, and D. J. Wineland, Phys. Rev. Lett. **77**, 4281 (1996). For theoretical work on state reconstruction for trapped ions, see R. L. de Matos Filho and W. Vogel, *ibid.* **76**, 4520 (1996); S. Wallentowitz and W. Vogel, *ibid.* **75**, 2932 (1995), J. F. Poyatos, R. Walser, J. I. Cirac, P. Zoller, and R. Blatt, Phys. Rev. A **53**, R1966 (1996); P. J. Bardroff, C. Leichtle, G. Schrade, and W. P. Schleich, Phys. Rev. Lett. **77**, 2198 (1996); C. D'Helon and G. J. Milburn, Phys. Rev. A **52**, 4755 (1995); C. D'Helon and G. J. Milburn, *ibid.* **54**, R25 (1996); C. D'Helon and G. J. Milburn, *ibid.* **54**, 5141 (1996).

[9] C. Monroe, D. M. Meekhof, B. E. King, and D. J. Wineland, Science **272**, 1131 (1996).

[10] W. M. Itano, C. Monroe, D. M. Meekhof, D. Leibfried, B. E. King, and D. J. Wineland, SPIE Proc. **2995**, 43 (1997).

[11] C. Monroe, D. M. Meekhof, B. E. King, W. Itano, and D. J. Wineland, Phys. Rev. Lett. **75**, 4714 (1995).

[12] J. I. Cirac and P. Zoller, Phys. Rev. Lett. **74**, 4091 (1995).

[13] D. F. V. James, Appl. Phys. B (to be published).

[14] S.-C. Gou and P. L. Knight, Phys. Rev. A **54**, 1682 (1996).

[15] S.-C. Gou, J. Steinbach, and P. L. Knight, Phys. Rev. A **54**, R1014 (1996).

[16] S.-C. Gou, J. Steinbach, and P. L. Knight, Phys. Rev. A **54**, 4315 (1996).

[17] C. C. Gerry, S.-C. Gou, and J. Steinbach, Phys. Rev. A **55**, 630 (1997).
[18] S.-C. Gou, J. Steinbach, and P. L. Knight, Phys. Rev. A **55**, 3719 (1997).
[19] W. K. Lai, V. Bužek, and P. L. Knight, Phys. Rev. A **43**, 6323 (1991).
[20] R. A. Fisher, M. M. Nieto, and V. D. Sandberg, Phys. Rev. D **29**, 1107 (1984); S. L. Braunstein and R. I. McLachlan, Phys. Rev. A **35**, 1659 (1987); M. Hillery, *ibid.* **42**, 498 (1990).
[21] G. Drobny and I. Jex, Phys. Rev. A **45**, 4897 (1992); V. Bužek and G. Drobny, *ibid.* **47**, 1237 (1993); G. Drobny, I. Jex, and V. Bužek, Acta Phys. Slov. **44**, 155 (1994); K. Banaszek and P. L. Knight, Phys. Rev. A **55**, 2368 (1997).
[22] H. Moya-Cessa, V. Bužek, M. S. Kim, and P. L. Knight, Phys. Rev. A **48**, 3900 (1993).
[23] D. J. Wineland (private communication).
[24] M. B. Plenio and P. L. Knight, Proc. R. Soc. London, Ser. A **452,** 1 (1997).
[25] S. A. Gardiner, J. I. Cirac, and P. Zoller, Phys. Rev. A **55**, 1683 (1997).
[26] A. Peres, *Quantum Theory: Concepts and Methods* (Kluwer Academic, London, 1993).
[27] S. Wallentowitz and W. Vogel, Phys. Rev. A **55**, 4438 (1997); G. S. Agarwal and J. Banerji, *ibid.* **55**, R4007 (1997).
[28] L. Allen and C. R. Stroud, Jr., Phys. Rep. **91**, 1 (1982).